Process monitoring and control strategies in extrusion-based bioprinting to fabricate spatially graded structures

Ashley A. Armstrong [a,*], Arielle Pfeil [a], Andrew G. Alleyne [a,b], Amy J. Wagoner Johnson [a,c,d]

[a] Mechanical Science and Engineering at The University of Illinois at Urbana Champaign, United States
[b] The Coordinated Science Laboratory, United States
[c] Carl R. Woese Institute for Genomic Biology, United States
[d] Carle Illinois College of Medicine, United States

ARTICLE INFO

ABSTRACT

Extrusion-based bioprinting is the most common printing technology used in regenerative medicine. Despite recent technological advances, a pressing challenge for extrusion printing is low spatial resolution, which limits the functionality of printed constructs. One of the reasons for the low spatial resolution is a lack of process monitoring and control strategies to monitor fabrication and correct for print errors. Few research efforts implement process control and investigate the relationship between extrusion process parameters and printing fidelity. The lack of understanding between process parameters and print results ultimately limits the complexity of the possible structures. For example, fabrication of structures whose topologies vary spatially within the part is not possible without advanced process control. Here we enable fabrication of advanced spatially graded structures by implementing process monitoring and control strategies. We develop material models to better understand the relationship between process parameters and printing outcomes. We also present an experimental procedure to generate a process map that provides insight into the regions of the processing space that produce the desired extrusion features (e.g., width of the filament). After generation of a process map and material models, we implement a process monitoring and control strategy that measures the feature error and intelligently updates the process control inputs to reduce defects and improve spatial fidelity, which will lead to better functionality of the final construct.

1. Introduction

Extrusion-based bioprinting is a three-dimensional (3D) printing method in which biomaterials, both cellular and acellular, with carefully tuned rheological properties are extruded through a nozzle using either a pneumatic or screw-driven force. During extrusion, a multi-axis motion system moves a nozzle along a pre-defined trajectory to fabricate structures in a layer-by-layer manner. Extrusion-based bioprinting is the most widely used printing technology in regenerative medicine [1,2] since it has the potential to rapidly fabricate human-scale tissue constructs [3,4] using biomaterials with high cell densities [5]. Extrusion printing has widespread applications in the biomedical field, including scaffold fabrication for tissue regeneration [6,7], organ printing [8–11], micro-vasculature printing [2], and disease modeling [12]. Despite recent technological advances, the fabrication of constructs that yield functional, mature tissues remains a major challenge in the field of regenerative medicine [13,14].

One of the reasons for the limited functionality of bioprinted constructs is low spatial resolution of the material extrusion process; depositing materials accurately is vital for in vivo functionality. For example, the geometry of the aortic valve is critical for ensuring efficient blood flow dynamics [15], coronary flow [16], and tissue durability [17]. This example demonstrates why tight control of material placement is essential to reproduce complex, hierarchical structures of native tissues with spatially varying feature sizes. Strategies to improve the accuracy of structure fabrication in extrusion printing are important to help realize the technology's clinical potential of printing human-scale, functional tissues [3,18–21].

The fabrication of functional tissue constructs requires a better understanding between printing process parameters and printing resolution [5]. Process mapping involves identifying the relationship between printing outcomes and the primary process variables to provide insight

---

into regions of the processing space that produce the desired printing outcome. While process mapping is common in machining and AM applications to improve print resolution [22,23], there are limited research efforts in the field of bioprinting that systematically investigate how process parameters affect fabrication [1,24,25]. Two examples of important process parameters for a pneumatic extrusion printing system include the speed of the axes and the pressure input, since both of these control inputs directly affect the amount of material extruded out of the nozzle. Examples of works where the researchers systematically studied how printing process parameters influence the process variable of interest include [1,5,25,26]. Some researchers have also developed models to relate the process parameters to printing outcomes [24,27].

While there are certainly research efforts investigating how process parameters affect print quality, the prior investigations determined a set of static process parameters, assuming a fixed set of optimized parameters would be utilized throughout the printing process. However, using constant process parameters can negatively impact the extrusion of the filament when the process itself is time varying. For example, significant material buildup can occur at regions with rapid deceleration to change directions, such as tight corners. Precise control of the filament width along more complicated paths requires process control and time varying process parameters to compensate for unavoidable material errors. He et al. increased the axis speed at tight corners to reduce material overlap [5]. The authors, however, simply doubled the speed in a region around the tight corner in an ad hoc manner and did not provide an explanation for how this adjustment was implemented. Further, this investigation did not present a means to measure or quantify material placement improvement at the sharp corner. Friedrich et al. developed a model to predict the deviation from the desired material path and ink spreading at corners to improve fabrication of tight corners in extrusion printing [28]. Despite these efforts, however, the field is currently lacking a method to implement correction based on process feedback.

The field also lacks a systematic method to select time varying process parameters to fabricate more complicated structures with spatially varying feature sizes such as filament widths. The references discussed above fabricate structures with a constant filament width along the path. Precise control of material placement for more complicated structures with varying filament widths requires process sensing and control, which involves measuring and quantifying material error, and then using the error intelligently to modify the control inputs to improve material fabrication.

This work expands on our previous research efforts to develop a process sensing and control methods that facilitate the selection of time varying process parameters and ultimately improve fabrication of structures with spatially varying features. Our previous work [29,30] focused on process control for structures with a constant filament width along the path. In this paper we outline the experimental steps required to develop a process map to provide insight into regions of the processing space that produce the desired printing outcome. We also present methods to determine both static and dynamic models of material fabrication to better understand how modifying process parameters affect fabrication. We then use information from the process map and models to facilitate selection and modification of process parameters that improve printing accuracy. We demonstrate the effectiveness of our approach by fabricating functionally graded scaffolds resulting in graded porosity patterns. An example application that could benefit from functionally graded porosity is fabrication of bone scaffolds, where the multiple porosity sizes could help direct bone growth and improve osseointegration. Other applications that require extruded material with varying widths along the trajectory include fabrication of organ substitutes *with complex internal geometries* [31,32] *and the coronary arterial tree that has branches with different size widths.* While we apply the method to a specific extrusion printing system, the steps outlined in this paper can be applied to other extrusion printing platforms to improve printing accuracy of complex parts with varying spatial features.

The paper is organized as follows. Section 2 presents the printing system we use for fabrication. The first step of the proposed method is presented in Section 3 which outlines the steps required to generate a process map that helps the user better understand the range of process parameters required to achieve the desired process variable of interest. Section 4 presents the experimental steps required to obtain both static and dynamic material models to quantify how modifying the process parameters affect the process variable. The material model information is then used in Section 5 to implement control design and generate a time varying input signal for the process parameters to fabricate a structure with spatially varying filament widths. In Section 6 we use this time varying control input for fabrication to demonstrate the effectiveness of the proposed method in printing functionally graded structures. Finally, Section 7 includes a discussion of the main contributions and future work.

2. Printing system

In this work we use a pneumatic-based extrusion printing system described in our previous work [18,30]. A pressure regulator applies a controlled pressure in the range of 0–30 psi to a syringe of material attached to an extruder head on the *Z*-axis of an *XYZ* motion system. We use a mapping from output pressure to input voltage to determine the voltage signal required to achieve the desired output pressure [33]. The motion system moves the extruder mount in the *XY* plane along the pre-defined trajectory, and a filament is deposited along the trajectory in the form of a cylindrical rod. For the current work, we use a general-purpose stainless-steel nozzle tip with a nozzle size (NS) internal diameter of 0.51 mm and a 6.35 mm tip length. We use an acellular calcium phosphate-based ceramic material system typical of applications in bone repair and regeneration [7,34]. The material is a yield-pseudoplastic fluid which behaves as a solid when unstressed and does not deform until a shear stress above the yield stress is achieved where the ink becomes shear-thinning [35].

The primary process variable of interest is the material filament width, Y (Fig. 1). Assuming a set nozzle size and material, the two process parameters we can modify to change the filament width include the pressure input signal, U_1, and the axis speed, U_2. With a constant speed, increasing the pressure will increase the width, while increasing the speed with a constant pressure will decrease the width.

To enable direct process control, we use a non-contact 2D laser displacement scanner (Keyence LJ-G030) that is mounted to the extruder head. The scanner measures both the spatial material placement and the width of the deposited material. We use the scanner output in a custom image processing script [18,30] to reproduce the surface profile and calculate the filament width error.

To validate the approach, we apply the process monitoring method to improve fabrication of two different two-layer square lattice patterns
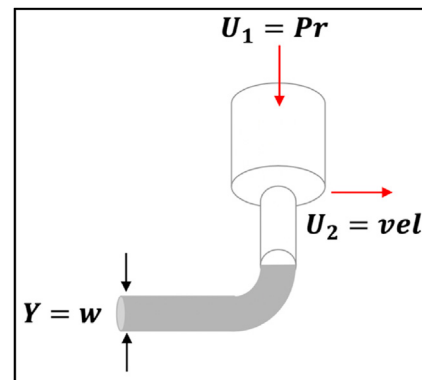

Fig. 1. The two process parameters we can vary in our printing system include the pressure input, U_1, and the axis speed, *vel*. The process variable of interest in this work is the filament width, Y. Image from Ref. [36].

with spatially varying features (Fig. 2). The reference designs have widths that vary from a size equal to the nozzle size (NS = 0.51 mm) to 1.75 times the NS to create functionally graded scaffold patterns. The patterns for Layers 1 and 2 of scaffold pattern 1 are the same with Layer 2 rotated 90° relative to Layer 1. The desired rods of each layer start at 1.75 times the NS on one side, reduce to the NS in the center, and then expand again to 1.75 times the NS on the other side, which is shown as the right filament on the right hand side of Fig. 2. The scaffold pattern has smaller pores on the outside with increasing pore size radially towards the center.

The pattern for Layer 1 of scaffold pattern 2 contains rods with widths equal to the NS on one end and grow to 1.75 times the NS on the other end, which is shown as the left filament on the right hand side of Fig. 2. Scaffold pattern 2 has smaller pores on the bottom of the scaffold, with increasing pore size towards the top.

3. Process map

This section presents a simple method to generate a process map to determine the range of feasible control inputs to achieve the desired fabrication outcome. The process map then guides the selection of the pressure inputs and speeds used in the subsequent sections. The experiment involves sweeping a range of pressure inputs and speeds and recording the resulting filament widths. The desired structures presented in Section 2 require filament widths in the range of the NS to 1.75 times the NS. Thus, our goal is to determine the combinations of pressures and speeds that lead to filament widths in this desired range.

The first step is to determine the range of process parameters that will be used in the process map experiments. For our material system, we choose to test a velocity range of 1–6 mm/s; from prior experience these axis speeds generally lead to stable extrusion and improved material adhesion to the substrate for our printing system [37]. The optimal pressure for extrusion, however, will vary depending on the viscosity of the material in an individual batch's formulation. Thus, we sweep across the entire 1–30 *psi* pressure input range.

To generate the process map, we then fabricate a series of straight lines. For each speed tested, a single axis moves the extruder along a straight line at a constant velocity. Every 5 mm the pressure input signal increases by 1 *psi* across the entire 1–30 *psi* pressure input range. After fabrication, the laser scanner moves across each filament and use a custom image processing script [30] to determine the resulting filament width. The resulting process map for our material system is illustrated in Fig. 3, which reports the filament width recorded as a factor of the NS, for each combination of pressure and velocity input. The color shading

represents the factor of the nozzle size with the scale bar on the right-hand side. The red and dark green regions on the left and right sides indicate unsuitable operating conditions. The pressure and velocity combinations that either do not lead to extrusion of continuous filaments or result in a filament width smaller than the NS are labeled as red squares. The velocity and pressure combinations that lead to a filament width that is larger than the desired filament width range are shown as dark green squares. The green color spectrum in the middle of the plot indicates the potential operating space for our application since the filament width is in the range of [NS, 1.75 NS]. The main purpose of the Process Map is to guide selection of operating parameters to achieve the desired filament width.

4. Material models

After generating a process map, the next step is to generate a material model to better understand how the material responds to control inputs in order to implement control design and ultimately improve material placement. We use the results of the Process Map to select the range of control inputs for the ink characterization experiments. Our experiments develop both static and dynamic material models that do not require extensive rheological information. The static material models relating the pressure and velocity inputs to the filament width are necessary to determine how to select the values of the initial input signals to fabricate structures with varying filament widths and how to modify the inputs for correction. The dynamic material models provide transient material information to help improve control design. We use established models in the literature and develop experiments to determine the model parameters.

4.1. Static material model

To determine the initial time varying process parameters, we use empirically determined curve fits. These static material models require both velocity and pressure experiments that are similar to the Process Map experiments, but with a smaller operating range. For the velocity experiments, we keep the pressure constant, and a single axis moves the extruder along a straight line. Every 5 mm, we increase the speed by 1 mm/s. Similarly, for the pressure experiments, a single axis moves the extruder along a straight line at a constant speed and we increase the pressure by 1 psi every 5 mm. The laser scanner and a custom image processing script [30] determine the resulting filament width.

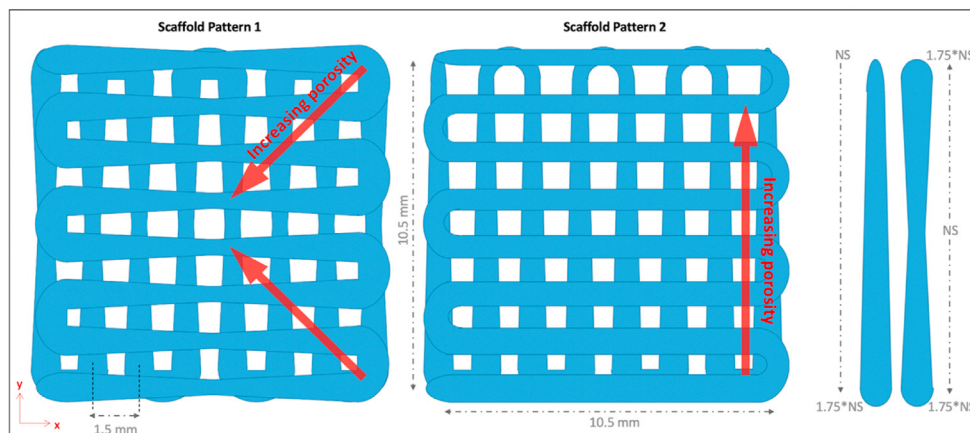We select the experimental pressure and speed ranges from the

Fig. 2. The two functionally graded scaffold patterns we print in this work to demonstrate the effectiveness of the proposed approach. The spatially varying filament widths create a graded scaffold pattern, indicated by the red arrows. Layers 1 and 2 for Scaffold pattern 1 use the same filament pattern, which is the filament pattern shown on the right side of the image where the width varies from 1.75 times the nozzle size (NS), to NS in the middle, and back to 1.75 times the NS on the far end. Layer 1 for Scaffold pattern 2 uses the filament width pattern where the width varies from the NS on one end to 1.75 times the NS on the other end. Layer 2 for Scaffold pattern 2 is a filament width that continuously increases along the path. The desired width at the starting point of Layer 2 is the NS, and the desired width at the end point of Layer 2 is 1.75 times the NS. (For interpretation of the references to color in this figure legend, the reader is referred to the Web version of this article.)
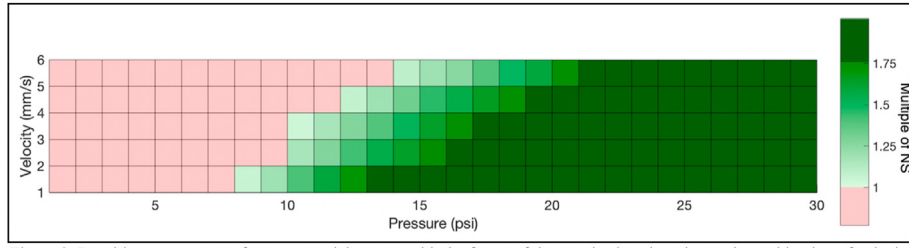
Fig. 3. Resulting process map for our material system with the factor of the nozzle size plotted at each combination of velocity and pressure inputs. The red region is the velocity and pressure combinations that do not result in continuous extrusion or lead to filament widths smaller than the NS. The middle green color spectrum is the desired printing region that results in filament widths in the desired range of NS – 1.75 times the NS. The dark green region indicates the velocity and pressure combinations where the filament width is larger than 1.75 times the NS. (For interpretation of the references to color in this figure legend, the reader is referred to the Web version of this article.)

Process Map results that resulted in filament widths in the desired 1–1.75 times the NS range. The experimental results for both the pressure and velocity tests are shown in Fig. 4. For the velocity and pressure tests, we choose a velocity range of 1–6 mm/s and test at three pressure values: 10, 13 and 16 *psi*, and a pressure range of 10–16 *psi* and test at three speeds: 2, 3 and 4 mm/s, respectively.

We fit the experimental data with standard curve fits (Fig. 4). The results from the velocity and pressure tests guide our selection for initial control design to enable fabrication of structures with varying filament widths. We can linearize Equation (4) around our operating region to enable control design. The linear fits for pressure are shown as solid lines in the right image of Fig. 4 and the average slope of the three experiments is $\overline{m} = 0.08$. This slope is used in Section 5 to implement control design for material correction. We also fit the velocity vs. width curves with lines in the typical 3–5 mm/s operating range to compare the slopes between the two control tools. The results in Fig. 4 demonstrate that in the operating space for fabrication, there is higher sensitivity with the pressure input, as seen by the slope of the linear fits, compared to the velocity input. The larger slopes of the pressure vs. width curves imply we have a larger control input sensitivity with the pressure input, which is discussed in Section 5.

4.2. Dynamic material model

We also design experiments to generate dynamic material models in order to determine information about transient material behavior. These models are important to improve control design for transient performance such as material flow starting and stopping [38]. We use a transfer function for the dynamic model, a mathematical model commonly used in control theory to represent the relationship between the output and input signals of a system [39]. One of the main advantages of transfer functions is that they use simple algebraic equations instead of complex differential equations for analyzing and designing systems. The transfer function is obtained by applying a Laplace transform to the differential

equations describing system dynamics and is written in the frequency domain using the complex variable, *s*. We use a linear first order approximation of extrusion dynamics to relate the input (pressure) and the output (volumetric flowrate at the nozzle), similar to Hoelzle et al. [38]. Hoelzle et al. model the ink dynamics by assuming a compressible ink in the syringe as a control volume with non-Newtonian fluid flowing through a nozzle [38]. The authors then linearized the dynamics about a nominal syringe volume resulting in the following linear first order transfer function to approximate the outflow response, $G(s)$:

$$G(s) = \frac{Q_{out}}{U}(s) = \frac{K}{\tau s + 1}e^{-\gamma s} \tag{1}$$

where Q_{out} is the output material flow rate and is equal to the product of the cross-sectional area of the extruded rod, A_{out}, and the axis printing speed, *vel*. For our application, the input, U, is the pressure signal applied to the ink syringe. The system gain, K, is the ratio of the magnitude of the steady-state step response to the magnitude of the step input; the time constant, τ, is the time it takes for the system's response to reach 63% of its steady-state value; and the extrusion delay, γ, is the time delay between when a signal is sent to the pressure regulator and when material starts extruding.

We present a time domain system identification experiment to identify the parameters of the first order approximation. System identification is a technique to build mathematical models of dynamic systems using measurements of the system's input and output signals [40]. The proposed system identification experiment involves two experimental tests. The first test is performed to approximate the extrusion mechanism delay. The reference trajectory for the first test is a straight line, single axis motion with length L and constant velocity. The pneumatic input is a pulse input with a constant pressure value *commanded to the pressure controller* for the entire movement (Fig. 5). The axis moves a distance L, but due to γ, the total filament length is less than L. We estimate the extrusion delay by comparing the total axis movement to the total length of the filament extruded, which is described in more detail in Ref. [30].
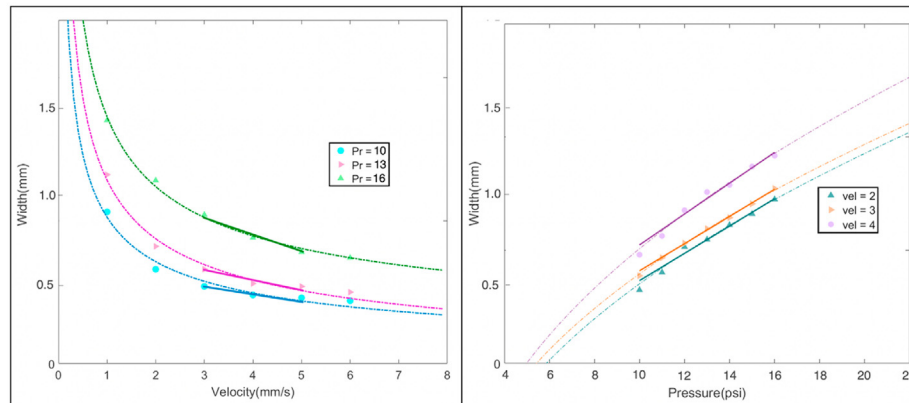

Fig. 4. Velocity (left) and pressure (right) tests to determine the relationship between control input modifications and material filament widths. The experimental data points are plotted as circles, arrows or triangles, and the dashed lines are the model fits. We fit the experimental data in our operating range with lines on the pressure vs. width image (right), to determine the slope which is used in material correction. We fit the velocity vs. width experimental data (left) in our typical printing speed operation range (3–5 mm/s) to compare slopes between the two curves.
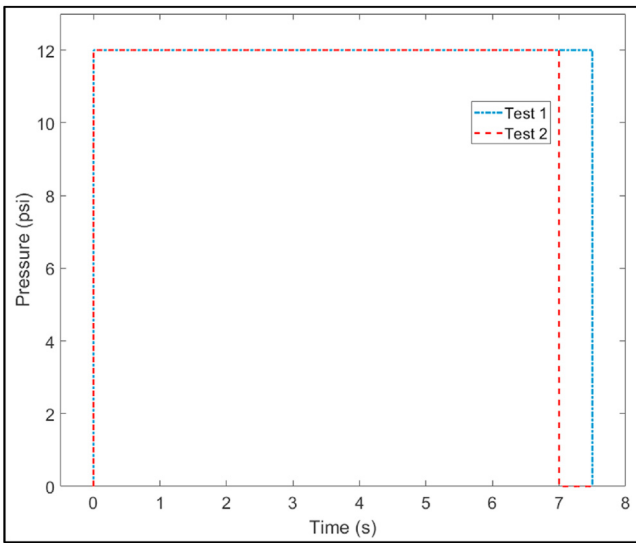
Fig. 5. Pressure input signals for the two system identification tests. The pressure is turned on for the entire 7.5 s motion for Test 1 to determine the material extrusion delay. The pressure is turned off 0.5 s before the end of motion in Test 2 to determine material drag.

The second test is similar to the first except the pressure input signal is shut off during the last 0.5 s of motion (Fig. 5). We use a 3x3 factorial design and perform both tests at three pressures ($Pr = 12, 13, 16\ psi$) and three speeds ($vel = 3, 4, 5\ mm/s$). We select the pressure and speed combinations from Fig. 4 that result in the desired filament width range. We measure the material behavior by scanning over the deposited filament with the laser scanner. In our previous work [30], we projected the laser scanner data onto the XY plane to determine the filament width. Here, we analyze the scanner data in the XZ plane to determine the cross-sectional area in order to calculate the volumetric flowrate. The ideal cross-sectional area, A_{ref}, is a circle with a radius equal to half the nozzle size. However, extrusion of yield-pseudoplastic material usually results in spreading after extrusion from a cylindrical nozzle [1]. For our material we choose to fit the XZ cross-section with an ellipse (Fig. 6), which is consistent with the literature for similar printing applications and material systems [41,42]. The cross-sectional area is computed as

$$A_{out} = \pi * a * b \tag{2}$$

where a and b are the major and minor axis of the ellipse. The custom image processing script steps through the scanner data along the Y axis and calculates Q_{out} by multiplying A_{out} by the axis speed for that particular experiment. We then use a built in MATLAB function called 'procest' to estimate the parameters of $G(s)$, which requires the experimental input and output data and assumed model structure as inputs. The input data is the pressure input signal, the output data is Q_{out}, and the assumed model structure is listed in (1). *The MATLAB scripts required for laser scanner data*

analysis are posted on GitHub under the following repository: 'aaarmst2/ process-control-bioprinting'.

The system identification results are shown in Fig. 7, which includes the first order system parameters determined by fitting the transfer function model in equation (5) to the experimental data. The purpose of Fig. 7 is to illustrate the results of the system identification tests and to compare the transfer function fits (solid line) to the experimental data (dots). The input and output gains are not necessarily the same for most systems, and the goal with control design is to design a controller such that the output of the system has the same gain as the input. In this paper, our method is iterative and improves the output behavior with each iteration.

The desired material flow rate is the product of the desired cross-sectional area, $A_{des} = \pi(\frac{NS}{2})^2$, and the printing speed: $Q_{ref} = A_{des}vel$. Both columns present the same data, but the left column fixes the speed and varies the pressure while the right column fixes the pressure and varies the speed.

The model responses, shown as solid lines, were calculated by using the transfer functions in simulation to determine the predicted response to different inputs (black dashed lines). The experimental data agrees well with the continuous time models and there are consistent patterns across all speeds and pressures. For the same speed, a larger input pressure results in a smaller extrusion delay, γ, a smaller time constant, τ, and a larger gain, K. For the same pressure, a larger speed results in a larger extrusion delay, a larger time constant, and a smaller gain.

5. Control design

While models certainly help with selection of initial control variables, modeling and control of extrusion dynamics is difficult due to the nonlinear behavior of yield-pseudoplastic fluids and challenges with process sensing. Relying solely on a material model may result in a final part with significant dimensional errors since the model can't precisely predict the material behavior during extrusion [43]. The material behavior varies between different batch manufacturing runs [33,38,43]. The uncertainty in material behavior necessitates the use of process control. In this section we outline the steps we perform to generate a time varying control input to achieve spatially varying filament width using the static material models. After initial fabrication of a part using this control input, we implement our process monitoring and control method [30] to further modify the control input and improve filament width control for the second round of fabrication.

5.1. Initial control input for iteration 1

The first step of control design requires the material information from the static material models presented in Section 4. Without control design, the user can only command a constant pressure input signal along the trajectory, shown as a gray solid line in Fig. 8. Control design using the material information from Section 4 enables us to intelligently vary the pressure input or axis speed along the trajectory to achieve varying filament width. In this work, we choose to keep the velocity constant
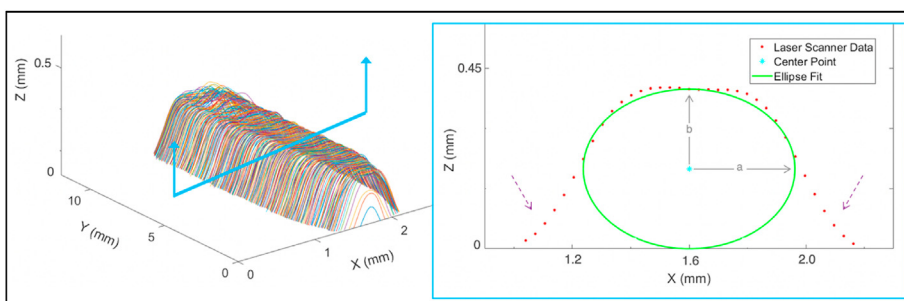

Fig. 6. Laser scanner data of a fabricated rod. Left: 3D laser scanner data. Right: cross-sectional area at a particular Y location. The laser scanner data is shown as red dotted lines, the center point is marked by a cyan blue asterisk, and the ellipse fit is shown in green. The ellipse is characterized by the major and minor axes, which are labeled as a and b, respectively. The sensor artifacts are highlighted by blue dashed arrows on either side of the ellipse fit. (For interpretation of the references to color in this figure legend, the reader is referred to the Web version of this article.)
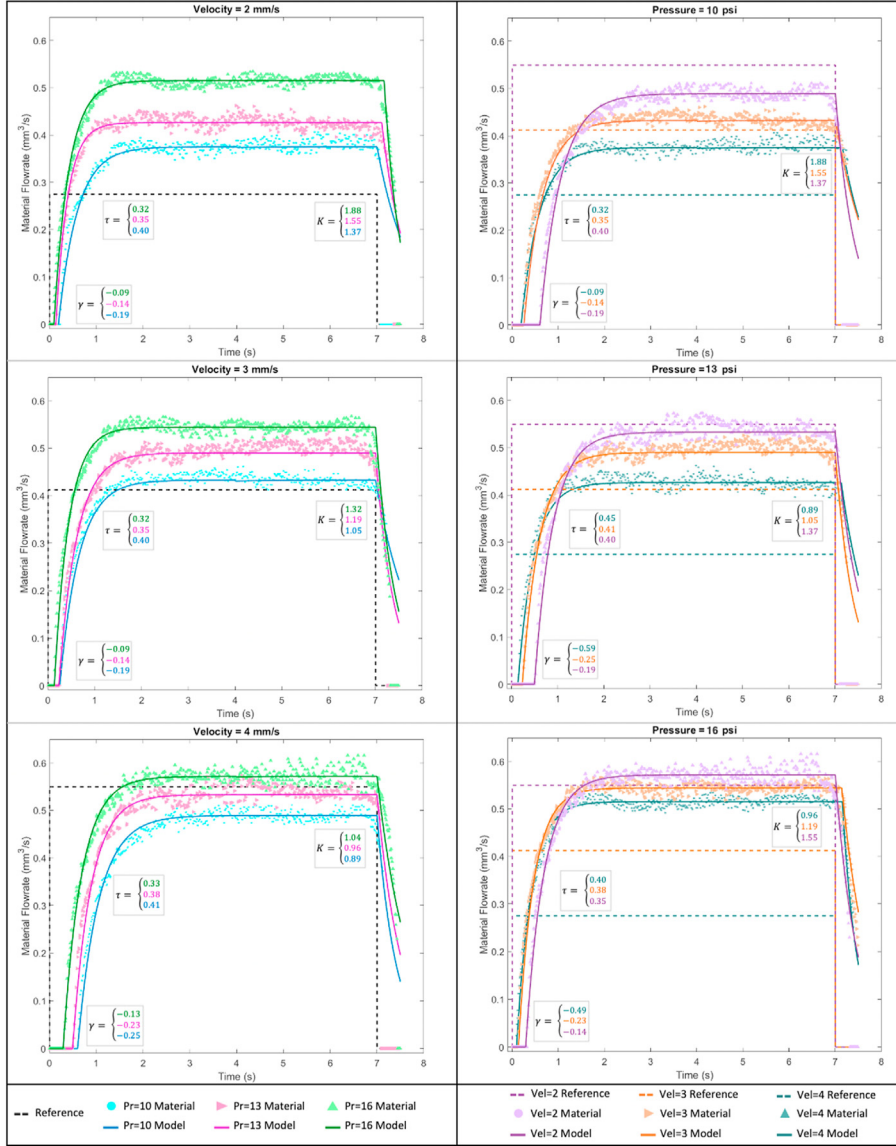
Fig. 7. System identification results comparing the experimental data with the model simulation for various speeds and pressures. The left column fixes the speed and varies the pressure. The right column fixes the pressure and varies the speed. The legends are at the bottom of each column. The experimental data are shown as circles, triangles and arrows. The model data, determined by simulation, are shown as solid lines. We include the desired material flow rate, Q_{ref}, as a dashed line on each of the figures. The three model parameters in Equation (1) are listed on each plot and are color coded. (For interpretation of the references to color in this figure legend, the reader is referred to the Web version of this article.)

throughout the trajectory and instead vary the pressure input for to control the filament width since the slopes of the pressure vs. width curves (Fig. 4) are larger than the velocity vs. width curves in our operating range (2–4 mm/s). The trends of the dynamic material models discussed in Section 4 are also more pronounced when we keep the speed constant and vary the pressure (Fig. 7). Both of these results imply we have more range of control of the rod width by using pressure as the input compared to velocity, which is consistent with other studies [1,5,25].

To fabricate the functionally graded scaffolds in Fig. 2, with filament widths between the NS to 1.75 times the NS, we select a printing speed of 3 mm/s and a pressure range of 10–15 *psi* based on the static material models in Fig. 4. The initial time varying pressure input signal used to fabricate iteration 0 for each layer pattern follows the desired time-varying width are shown in Fig. 8. We use the initial time-varying pressure input signals, which are shown as black dashed lines, to fabricate iteration 1 of each scaffold pattern. We discuss how we determine the modified control inputs for fabrication of iteration 2, which are shown as red lines, in the next subsection.

5.2. Material correction for iteration 2

The static material models provide starting points for the original

pressure inputs for each scaffold pattern. However, additional process control and material correction is required to monitor material behavior during fabrication due to the nonlinear material behavior, and since fabrication patterns like tight angles or turnarounds can cause material buildup. The main goal of our technique is to use the process feedback from the laser scanner to modify the control inputs and achieve the as-designed, spatially varying filament width. Process control enables us to correct for regions with material overbuild or underbuild by decreasing or increasing the pressure.

After fabrication of iteration 1 using the original pressure input signals shown in Fig. 8, we implement the process monitoring and control tool presented in Ref. [30] for material correction and to further improve filament width control. We calculate the filament width error by comparing the scanner data to the desired spatially varying filament width. We then modify the pressure input in proportion to the width error to determine the pressure input for iteration 2 using the material information from Section 4:

$$P_2(t) = P_1(t) + \overline{m} e_w(t + \gamma), \tag{3}$$

where $P_2(t)$ is the time varying pressure input for iteration 2, $P_1(t)$ is the pressure input for iteration 1, $\overline{m}$ is the slope of the pressure vs. width
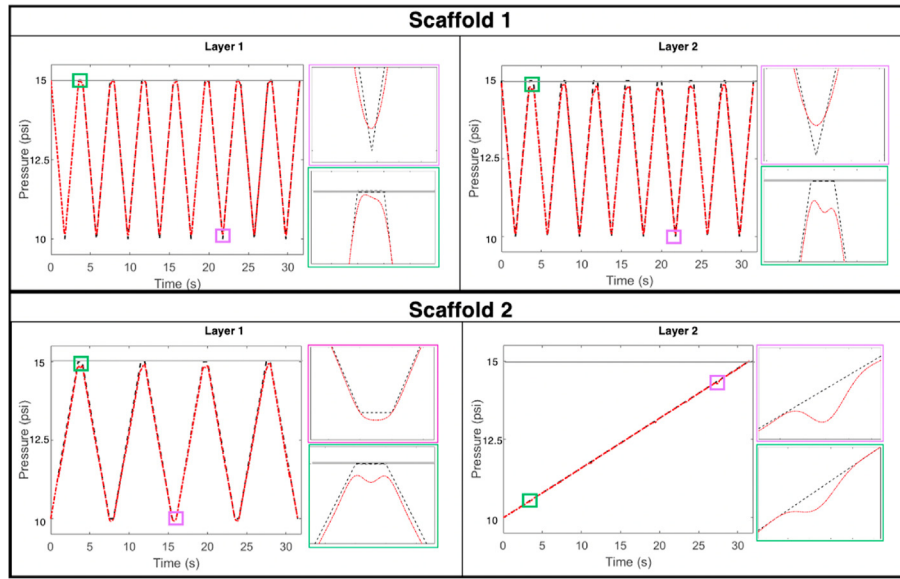
Fig. 8. Pressure input signals for iterations 0, 1 and 2. Scaffold 1 and Scaffold 2 refer to the functionally graded scaffolds in Fig. 2. The constant pressure input signal for fabrication of iteration 0 is a gray solid line, ——, the pressure input signal for iteration 1 is a black dashed line, - - - , and the pressure input signal for iteration 2 is a red solid line, ——. The pressure input signal for Layers 1 and 2 for Scaffold Pattern 1 are the same and are shown in the top row as black dashed lines. The pressure input signals for Layers 1 and 2 for Scaffold Pattern 2 are shown in the bottom row also shown as black dashed lines. (For interpretation of the references to color in this figure legend, the reader is referred to the Web version of this article.)

static material model in Fig. 4, $e_w(t)$ is the width error, t is the time duration, and γ is the material extrusion delay from the dynamic material model presented in Section 4. P_1 for each layer pattern is shown as black dashed lines and P_2 for each layer pattern is shown as red solid lines in Fig. 8. The slope of the pressure static material model, $\overline{m}$, is used to convert the filament width error in mm to units of psi, which is then added to the existing pressure input signal. We also use the material extrusion delay, γ, from the dynamic material models (Fig. 6) to determine at what time the pressure input signal should be reduced so that the error correction occurs at the correct location. Thus, the adjustments in the pressure input signal are shifted back in time by γ seconds to compensate for the material extrusion delay. Between iterations 2 and 1 we modify the pressure inputs based on the performance of the previous iteration,

which helps compensate for model uncertainty [44]. The modified pressure input signal is shown as a red line in Fig. 8, and the insets demonstrate that we reduce the pressure input at turnarounds to reduce the amount of material buildup. The results of implementing this correction are presented in Section 6.

6. Printing results

To demonstrate the effectiveness of the proposed method, we fabricate the functionally graded scaffold patterns illustrated in Fig. 2. The fabricated scaffolds for Scaffold Patterns 1 and 2 are shown in Fig. 9. All scaffolds include lead-in lines before the start of the scaffold in order to improve material flow during printing and to get rid of any possible air
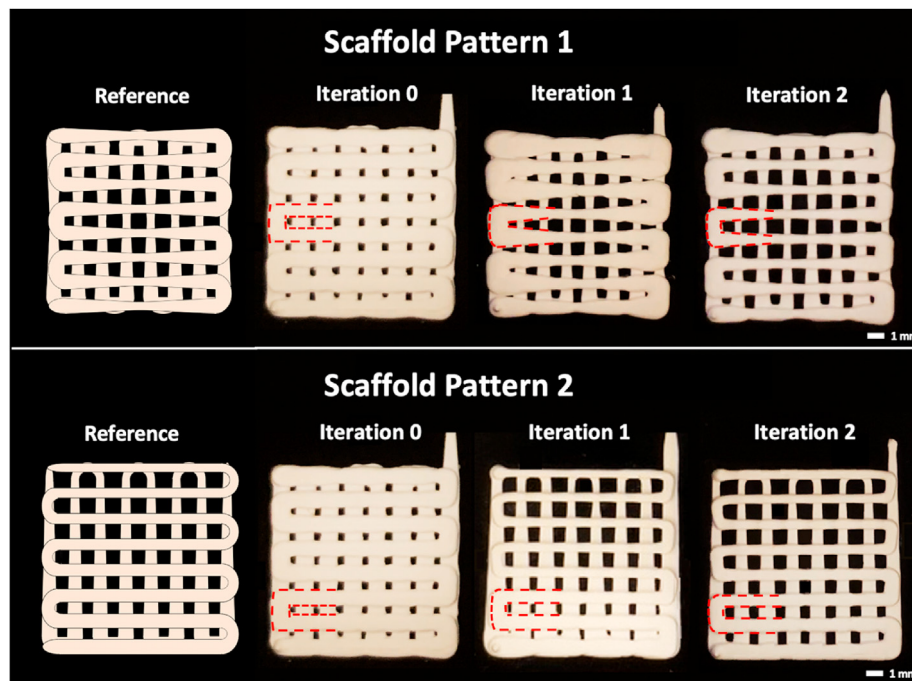

Fig. 9. Fabricated scaffold patterns. Iteration 0 is the fabricated pattern with a constant pressure signal. Iteration 1 is the fabricated pattern with a time varying pressure signal. Iteration 2 is the fabricated pattern after implementation of the process monitoring and control method to adjust the pressure input to improve material fabrication. Each scaffold pattern contains a lead in line before starting the print.

bubbles. The scaffolds labeled as 'Iteration 0' are the patterns fabricated without process control using the constant pressure input signal shown as a gray solid line in Fig. 5. The scaffolds labeled as 'Iteration 1' are the patterns fabricated with the initial control design using the time varying pressure input signals shown as black dashed lines in Fig. 5. Finally, the scaffolds labeled as 'Iteration 2' are the patterns fabricated after implementation of process monitoring and control using the modified pressure input signals shown as red solid lines in Fig. 5. The modified pressure input, $P_2(t)$, compensates for the material overbuild by reducing the pressure input at these regions.

The filament width error is calculated point wise in space along the reference trajectory [30]. There is significant improvement between iterations 0 and 1 for both scaffold patterns. For Scaffold Pattern 1, there is more width error for iteration 1 in Layer 2 relative to Layer 1. Thus, the pressure signal for Layer 2 is reduced more than the pressure signal for Layer 1 (Fig. 8). For Scaffold Pattern 2, there is more width error for iteration 2 in Layer 1 relative to Layer 2. Thus, the pressure signal for Layer 1 is reduced more than the pressure signal for Layer 2 (Fig. 8). After implementation of the process monitoring and control method, there is additional improvement in filament width control between iterations 1 and 2 for both scaffold patterns which results in more precisely defined porosity patterns.

To quantify the filament width control improvement between iterations and to assess the accuracy of the printed parts, we use the two-norm of the filament width error, e_{w,it_2}, to evaluate the size of the error vectors. A reduction in the two-norm implies less overall filament width error throughout the part. Comparing iterations 0 and 1, there is a 76% and 71% reduction in the error two-norm for Scaffold patterns 1 and 2, respectively. Comparing iterations 1 and 2, there is an additional 32% and 28% reduction in the error two-norm for Scaffold patterns 1 and 2, respectively.

To compare filament width improvement between iterations, we define the error differential, E_{it}, as:

$$E_{it} = e_{w,it} - e_{w,it-1},$$

where $e_{w,it}$ is the filament width error at a given iteration, it. For example, E_2 is defined as $E_2 = e_{w,2} - e_{w,1}$ and defines the error improvement between iterations 2 and 1. The steps to determine the filament width error are discussed in detail in Ref. [30]. The magnitude of the error differential between iterations 0 and 1 and iterations 1 and 2 are plotted spatially along the reference trajectories of each layer in Fig. 10. The color shading shows the magnitude of the error differential at each point on the reference trajectory with the scale bar on the right-hand side, where a darker red color indicates a larger error improvement. The plots in the *top row* demonstrate there is significant improvement between iterations 0 and 2. The plots in the *bottom row* demonstrate the additional improvements after application of the process monitoring and control method between iterations 1 and 2.

7. Discussion & conclusion

The accuracy of current bioprinting methods is limited due to a lack of process monitoring and control methods to monitor fabrication and correct for defects. A better understanding between process parameters and printing outcomes improves printing accuracy. This work presents simple ink characterization experiments to generate a process map in order to investigate the relationship between two printing parameters, pressure input and print speed, and the width of the filament extruded through a nozzle. We also present two methods to develop static and dynamic material models that include material properties required for control design. We modify models from the literature and demonstrate how they can be implemented in practice to improve control design. The method presented in this work enables a new level of complexity in filament fabrication which is important for regenerative medicine since tissues have complex and hierarchical structures.

The static material models approximate how changes in the pressure and velocity inputs affect the filament width. The results (Fig. 4) are consistent with previous studies [25] where the filament width decreased with increasing deposition speed and decreasing pressure. Moreover, the shape of the velocity curve, which implies the velocity input has a smaller sensitivity relative to the pressure input, is similar to the results presented in Refs. [1,5,25]. Similar to Ref. [25], our material system demonstrates a higher sensitivity with the pressure input. Thus, for control design we choose to keep the velocity constant and vary the pressure input to control the filament width. The data from the pressure vs. width curve guides the initial design of the time-varying pressure inputs to fabricate iteration 1 of the functionally graded scaffolds.

We use information from both the static and dynamic material models to implement process control. We use the slope of the pressure vs. width curve, $\overline{m}$, to convert the filament width error in units of *mm* to units of *psi* to generate the modified pressure input, $P_2(t)$, for fabrication of iteration 2. The dynamic material models provide three pieces of information about the material during fabrication for a given pressure and velocity input: the gain, K, the time constant, τ, and the extrusion delay, γ. We use two of these parameters, K and γ, since the system gain is related to the slope of the pressure vs. width curves and the extrusion delay determines at what time we should modify the pressure input signal. The slope of the static model, $\overline{m}$, then determines how much we should modify the pressure input signal. Using two of the three model parameters in the process and control step was sufficient to improve material fabrication with a 32 and 28% reduction in filament width error between iterations 2 and 1 for Scaffold Patterns 1 and 2, respectively. Future work will incorporate the time constant into the process control method. Compensating for the time constant with control design, for example, can help improve regions with sharp transitions between regions with small and large widths. The time constant can also be used as a means to evaluate or improve new materials for fabrication. Future will also use the extrusion delay and time constant to improve the start and stop of ink extrusion, which would remove the lead in lines from fabricated structures.

In this work we used linear material models for both the static and dynamic models to approximate the nonlinear material behavior. There are more complicated, nonlinear models in the literature, but nonlinear models are not conducive to simple control design. The addition of process sensing and control helps correct for some of the inherent modeling error with linear models.

This study presents the concept and methodology, and we demonstrated process improvement for a calcium-phosphate based material system. Future work could apply the method using different materials with detailed rheological data to compare the efficacy across a wider range of materials.

This work uses a non-contact laser scanner to enable process sensing. The sensing process and data collection are relatively simple and quick. There are, however, limitations in the sensor's capabilities. The laser scanner uses the principle of triangulation to reproduce the surface profile. The scanner projects a laser sheet on the target object, and the light reflected back to the scanner is mapped onto a light-receiving element to determine the object's distance from the scanner. Since the extruded filament is cylindrical, the bottom of the cross-sectional ellipse cannot be measured and the scanner data includes sensor artifacts on either side of the ellipse (Fig. 6). We confirmed the artifacts by scanning over a circular rod with a known circular cross section and the data had the tails present on both sides (data not shown). We compensate for this sensing limitation by fitting the data with an ellipse.

In addition to the iteration-to-iteration process outlined in this work, the laser scanner data could be used as direct feedback within each iteration to respond to deviations from the intended print trajectory and iteration varying disturbances. The coupling of this in-situ process monitoring and the iteration-to-iteration correction would further enhance the spatial material placement. This coupling and real-time process control, however, requires additional data processing and
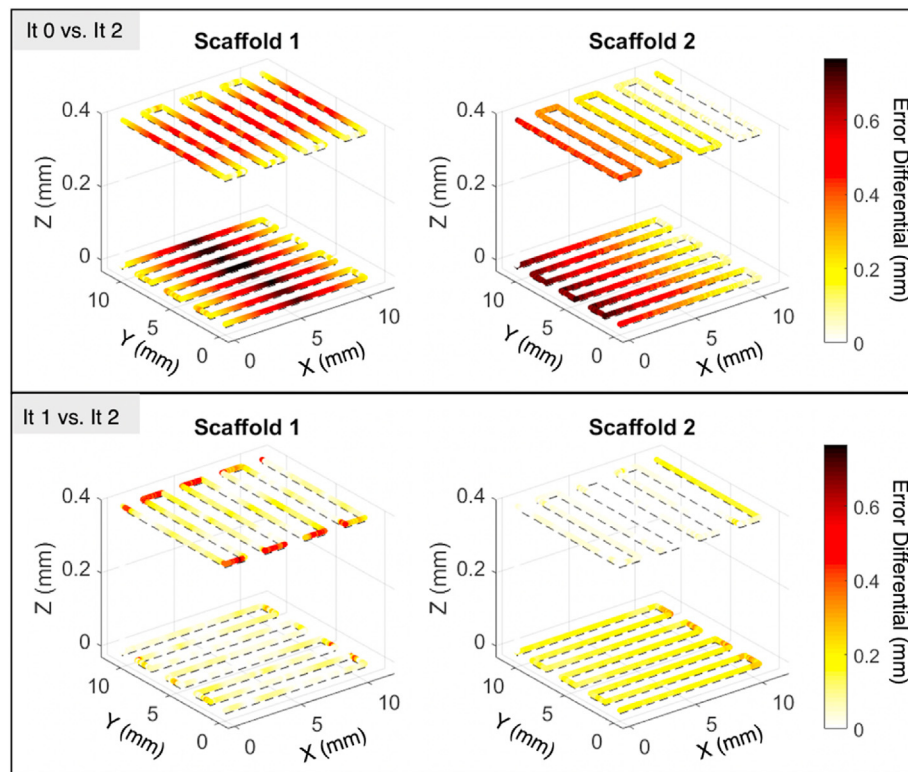
Fig. 10. Error differential plots comparing iteration 0 to iteration 2 (top row) and iteration 1 to iteration 2 (bottom row). The magnitude of the error differential at each point on the reference trajectory is presented as a color shading with the scale bar on the right side. A darker color represents a larger magnitude implying a larger improvement at that specific location. (For interpretation of the references to color in this figure legend, the reader is referred to the Web version of this article.)

implementation complexity outside the scope of the current work.

In conclusion, instead of relying on rheological data, we present experiments to determine a process map and material models to better understand how modifying the process parameters affect the material filament width. We then use the material models in control design to enable precise fabrication of parts with spatially varying widths. We implement process control to improve filament width control throughout the part. Critical locations such as tight corners need more effort to identify the proper changes in process parameters to avoid excessive accumulation of material in those areas.

While we apply the method to a specific extrusion printing system, the steps outlined in this paper can be applied to other extrusion printing platforms in order to improve printing accuracy of complex parts with varying filament widths. Researchers can perform the experiments in Section 4 with their material to determine the relationship between printing parameters and the process variable of interest and thus determine the range of feasible control inputs. Accurate filament deposition requires a way to infer what the machine settings should be in order to achieve the desired material behavior. The experiments presented in this work provide information that will help guide the selection of time-varying control inputs to enable fabrication of more advanced structures with spatially varying features.

CRediT authorship contribution statement

Ashley A. Armstrong: Conceptualization, Methodology, Software, Investigation, Writing - original draft. **Arielle Pfeil:** Resources. **Andrew G. Alleyne:** Conceptualization, Writing - review & editing, Supervision, Project administration, Funding acquisition. **Amy J. Wagoner Johnson:** Conceptualization, Writing - review & editing, Supervision, Project administration, Funding acquisition.

Declaration of competing interest

The authors declare that they have no known competing financial interests or personal relationships that could have appeared to influence the work reported in this paper.

Acknowledgements

References

[1] E. Sodupe-Ortega, A. Sanz-Garcia, A. Pernia-Espinoza, C. Escobedo-Lucea, Accurate calibration in multi-material 3D bioprinting for tissue engineering, Materials 11 (8) (2018) 1–19.

[2] W. Wu, A. Deconinck, J.A. Lewis, Omnidirectional printing of 3D microvascular networks, Adv. Mater. 23 (24) (2011) 178–183.

[3] M.H. Ibrahim, T. Ozbolat, Current advances and future perspectives in extrusion-based bioprinting, Biomaterials 76 (2016) 321–343.

[4] L. Ning, X. Chen, A brief review of extrusion-based tissue scaffold bio-printing, Biotechnol. J. 12 (8) (2017).

[5] Y. He, F. Yang, H. Zhao, Q. Gao, B. Xia, J. Fu, Research on the printability of hydrogels in 3D bioprinting, Sci. Rep. 6 (2016) 1–13.

[6] Y. Xie, et al., Net shape fabrication of calcium phosphate scaffolds with multiple material domains, Biofabrication 8 (1) (2016), 015005.

[7] L.E. Rustom, et al., Multiscale porosity directs bone regeneration in biphasic calcium phosphate scaffolds, ACS Biomater. Sci. Eng. 3 (11) (2017) acsbiomaterials.6b00632.

[8] T. Hinton, Q. Jallerat, E. Al, Three-dimensional printing of complex biological structures by freeform reversible embedding of suspended hydrogels, Sci. Adv. 1 (9) (2015), e1500758.

[9] B. Duan, L. Hockaday, K. Kang, J. Butcher, 3D bioprinting of heterogeneous aortic valve conduits with alginate/gelatin hydrogels 101 (5) (2013) 1255–1264.

[10] A. Isaacson, S. Swioklo, C.J. Connon, 3D bioprinting of a corneal stroma equivalent, Exp. Eye Res. 173 (2018) 188–193.

[11] C.S. Ong, et al., Creation of cardiac tissue exhibiting mechanical integration of spheroids using 3D bioprinting, J. Vis. Exp. 125 (2017) 2–6.

[12] M.A. Heinrich, R. Bansal, T. Lammers, Y.S. Zhang, R. Michel Schiffelers, J. Prakash, 3D-Bioprinted mini-brain: a glioblastoma model to study cellular interactions and therapeutics, Adv. Mater. 1806590 (2019) 1–9.

[13] R. Levato, T. Jungst, R. G. Scheuring, T. Blunk, J. Groll, and J. Malda, "From shape to function: the next step in bioprinting," Adv. Mater., vol. 1906423, 2020.

[14] X. Wang, B.L. Rijff, G. Khang, A building-block approach to 3D printing a multichannel, organ-regenerative scaffold, J. Tissue Eng. Regen. Med. 11 (5) (2017) 1403–1411.

[15] B. Bellhouse, F. Bellhouse, Fluid mechanics of the aortic root with application to coronary flow, Nature 219 (5158) (1968) 1059–1061.

[16] I. Vesely, Aortic root dilation prior to valve opening explained by passive hemodynamics, J Hear. Valve Dis. 9 (1) (2000) 16–20.

[17] P. Dagum, G. Green, E. Al, Deformational dynamics of the aortic root: modes and physiologic determinants, Circulation1 100 (19 Suppl) (1999) II54–62.

[18] A. Armstrong, J. Norato, A. Alleyne, A. Wagoner Johnson, Direct process feedback in extrusion-based 3D bioprinting, Biofabrication 12 (1) (2019).

[19] S. Vijayavenkataraman, W.C. Yan, W.F. Lu, C.H. Wang, J.Y.H. Fuh, 3D bioprinting of tissues and organs for regenerative medicine, Adv. Drug Deliv. Rev. 132 (2018) 296–332.

[20] T.J. Hinton, A. Lee, A.W. Feinberg, 3D bioprinting from the micrometer to millimeter length scales: size does matter, Curr. Opin. Biomed. Eng. 1 (2017) 31–37.

[21] S. V Murphy, A. Atala, 3D bioprinting of tissues and organs, Nat. Biotechnol. 32 (8) (2014) 773–785.

[22] K. Aoyagi, H. Wang, H. Sudo, A. Chiba, Simple method to construct process maps for additive manufacturing using a support vector machine, Addit. Manuf. 27 (2019) 353–362. October 2017.

[23] J. Gockel, J. Beuth, Understanding Ti-6Al-4V Microstructure Control in Additive Manufacturing via Process Maps Joy Gockel and Jack Beuth Department of Mechanical Engineering, Carnegie Mellon University, Solid Free. Fabr. Proc., Pittsburgh, PA, 2013, pp. 666–674, 15213.

[24] R. Suntornnond, E.Y.S. Tan, J. An, C.K. Chua, A mathematical model on the resolution of extrusion bioprinting for the development of new bioinks, Materials 9 (9) (2016).

[25] J.E. Trachtenberg, et al., Extrusion-based 3D printing of poly(propylene fumarate) in a full-factorial design, ACS Biomater. Sci. Eng. 2 (10) (2016) 1771–1780.

[26] L. Friedrich, M. Begley, In situ characterization of low-viscosity direct ink writing: stability, wetting, and rotational flows, J. Colloid Interface Sci. 529 (2018) 599–609.

[27] T. Guo, T. Holzberg, C. Lim, F. Gao, E. Al, 3D printing PLGA: a quantitative examination of the effects of polymer composition and printing parameters on print resolution, Biofabrication 9 (2) (2018).

[28] L. Friedrich, M. Begley, Corner accuracy in direct ink writing with support material, Bioprinting 19 (2020).

[29] A. Armstrong, J. Norato, A. Wagoner Johnson, A. Alleyne, Direct process feedback in extrusion-based 3D bioprinting, Biofabrication (2019).

[30] A. Armstrong, A. Alleyne, A. Wagoner Johnson, 1D and 2D error assessment and correction for extrusion-based bioprinting using process sensing and control strategies, Biofabrication (2020).

[31] A. Atala, Engineering organs, Curr. Opin. Biotechnol. 20 (5) (2009) 575–592.

[32] L. Liu, X. Zhou, Y. Xu, W. Zhang, E. Al, Controlled release of growth factors for regenerative medicine, Curr. Pharmaceut. Des. 21 (12) (2015).

[33] A. Armstrong, A. Wagoner Johnson, A. Alleyne, Modeling and Control of an Easy-To-Use Direct Write Printing System for Fabrication of Bone Scaffolds, " University of Illinois at Urbana Champaign, 2017.

[34] D. Hoelzle, S. Svientek, A. Alleyne, A.W. Johnson, Manufacturing controls for the fabrication of tissue scaffolds with graded microstructures, in: Materials Science and Technology, MS&T, 2011, pp. 1469–1476.

[35] R. Chhabra, J.F. Richardson, Non-Newtonian Flow in the Process Industries, Butterworth-Heinemann, Oxford, UK, 1999.

[36] A. Armstrong, A. Alleyne, A Multi-Input Single-Output Iterative Learning Control for Improved Material Placement in Extrusion-Based Additive Manufacturing, *Control Eng. Pract.*, 2020.

[37] D.J. Hoelzle, S.R. Svientek, A.G. Alleyne, A.J. Wagoner Johnson, Design and manufacture of combinatorial calcium phosphate bone scaffolds, J. Biomech. Eng. 133 (10) (2011) 101001.

[38] D.J. Hoelzle, A.G. Alleyne, A.J. Wagoner Johnson, Iterative Learning Control for Robotic Deposition Using Machine Vision, Am. Control Conf., 2008, pp. 4541–4547, 2008.

[39] G. Goodwin, S. Graebe, M. Salgado, Control System Design, Pearson, 2000.

[40] L. Ljung, System Identification: Theory for User, PTR Prentice Hall, Englewood Cliffs, New Jersey, 1987.

[41] D.J. Hoelzle, Reliability Guidelines and Flowrate Modulation for a Micro Robotic Deposition System, University of Illinois at Urbana-Champaign, 2007.

[42] J. Cesarano, R. Segalman, P. Calvert, Robocasting provides moldless fabrication from slurry deposition, Ceram. Ind. 148 (4) (1998) 94–102.

[43] A. Simeunovic, D. Hoelzle, Nonlinear and linearized gray box models of direct-write printing dynamics, in: Solid Freeform Fabrication Symposium, 2018.

[44] K.L. Moore, Y.C.Y. Chen, H.-S.A.H.-S. Ahn, Iterative learning control: a tutorial and big picture view, in: Proc. 45th IEEE Conf. Decis. Control, Ilc, 2006, pp. 2352–2357.